Characterization and Structure-Property Relationships of an Injectable Thiol-Michael Addition Hydrogel Toward Compatibility with Glioblastoma Therapy

Zerin Mahzabin Khan^a, Emily Wilts^b, Eli Vlaisavljevich^a, Timothy E. Long^c, and Scott S. Verbridge^{a*}

^aVirginia Tech – Wake Forest University School of Biomedical Engineering and Sciences, Virginia Tech, Blacksburg, VA 24061, USA

^bDepartment of Cellular and Physiological Sciences, University of British Columbia, Vancouver, BC V6T 1Z3, CA

^cBiodesign Center for Sustainable Macromolecular Materials and Manufacturing, Arizona State University, Tempe, AZ 85287, USA

*Corresponding Author Scott S. Verbridge Virginia Polytechnic Institute and State University Department of Biomedical Engineering and Mechanics 345 Kelly Hall, 325 Stanger St., Blacksburg, VA 24061

Email: <u>sverb@vt.edu</u> Phone: (540) 231-2908

Abstract

Glioblastoma multiforme (GBM) is an aggressive primary brain cancer and although patients undergo surgery and chemoradiotherapy, residual cancer cells still migrate to healthy brain tissue and lead to tumor relapse after treatment. New therapeutic strategies are therefore urgently needed to better mitigate this tumor recurrence. To address this need, we envision after surgical removal of the tumor, implantable biomaterials in the resection cavity can treat or collect residual GBM cells for their subsequent eradication. To this end, we systematically characterized a poly(ethylene glycol)-based injectable hydrogel crosslinked via a thiol-Michael addition reaction by tuning its hydration level and aqueous NaHCO₃ concentration. The physical and chemical properties of the different formulations were investigated by assessing the strength and stability of the polymer networks and their swelling behavior. The hydrogel biocompatibility was assessed by performing in vitro cytotoxicity assays, immunoassays, and immunocytochemistry to monitor the reactivity of astrocytes cultured on the hydrogel surface over time. These characterization studies revealed key structure-property relationships. Furthermore, the results indicated hydrogels synthesized with 0.175 M NaHCO₃ and 50 wt% water content swelled the least, possessed a storage modulus that can withstand high intracranial pressures while avoiding a mechanical mismatch, had a sufficiently crosslinked polymer network, and did not degrade rapidly. This formulation was not cytotoxic to astrocytes and produced minimal immunogenic responses in vitro. These properties suggest this hydrogel formulation is the most optimal for implantation in the resection cavity and compatible toward glioblastoma therapy.

Keywords: glioblastoma, astrocytes, thiol-Michael addition, injectable hydrogel, characterization

1. Introduction

Glioblastoma multiforme (GBM) is the most aggressive and common primary brain tumor in adults. Poorly defined borders make complete resection of the primary tumor mass difficult, and adjuvant chemotherapy and radiotherapy are subsequently administered to eradicate the remaining cancer cells and prevent tumor recurrence. However, permeation of chemotherapeutic drugs is limited by the blood-brain-barrier, while the doses of radiotherapy often lead to healthy tissue necrosis [1]. Even with combinatorial therapies, residual GBM cells invade the healthy brain parenchyma by traveling through white matter tracts and blood vessels to form secondary tumors within 2 – 3 cm of the original resection cavity in 90% - 95% of patients, whose median survival times are only 15 months [2]. A subpopulation of GBM cells with stem cell-like properties known as glioma stem cells (GSCs) initiate tumor growth and resist conventional therapy [3], yet the lack of consensus on their established surface biomarkers make selective targeting of GSCs difficult [4]. Strategies to effectively eliminate these heterogeneous populations of GBM are urgently needed to mitigate tumor recurrences while minimizing damage to the brain.

Most GBM research focuses on targeted therapies to eradicate the malignant cells. Although localized treatments like biodegradable wafers loaded with chemotherapeutic agents that release drugs in the resection cavity have been tested on patients, randomized clinical studies did not yield improved outcomes [1]. Recently, techniques have been developed to attract GBM cells by harnessing their infiltrative capacity and guiding cancer cell migration to implants for their subsequent eradication. For example, Autier and colleagues developed a cellulose-based hydrogel to release chemokines in the resection bed to attract and immobilize GBM cells on the implant [5]. However, the hydrogel was not biodegradable and the chemotactic gradient was diffusion limited to 5 mm. Polycaprolactone nanofibers have also been developed to mimic

blood vessels and white matter tracts and guide GBM cells to an extracortical, drug-conjugated hydrogel to induce apoptosis [6]. Yet, this conduit is highly invasive and can potentially leak tumor cells into healthy brain tissue if compromised. We are developing a hydrogel-based treatment that can address these limitations, and the specific aim of this present study is to optimize the hydrogel formulation for compatibility with the GBM microenvironment. For the future GBM treatment approach, we envision that this optimized hydrogel can be injected into the GBM resection cavity to crosslink *in situ* and conform to patient specific anatomy. A combination of chemical and physical cues, such as chemotaxis [6] and electrotaxis [7], can then selectively guide GBM/GSC migration into the hydrogel to entrap the malignant cells. An ablation technique, such as focused ultrasound [8] can then potentially enable the non-invasive ablation of the entrapped cancer cells. Specifically, we envision histotripsy can be employed to non-thermally and mechanically fractionate GBM cells to an acellular debris and liquid homogenate [9] with precise lesion areas [10].

This study focused on characterizing the injectable hydrogel to deduce key structureproperty relationships and tune the hydrogel toward compatibility with glioblastoma therapy.

Click chemistry refers to reactions in which the reagents rapidly crosslink, produce high yields, and are not impacted by water and biological processes *in vivo* due to their bio-orthogonal nature [11]. Click reactions are therefore suitable for synthesizing injectable materials, and more specifically, the thiol-Michael addition reaction can occur under physiological temperatures and pH [12] and is ideal for generating hydrogels that encapsulate proteins and cells [13]. The thioether linkage in thiol-acrylate reactions can be hydrolytically degraded, while bases are efficient thiol-Michael addition catalysts that minimize side reactions [14]. The alkaline environment deprotonates thiol groups to produce nucleophilic thiolate anions and conjugate

acids [14]. The thiolate anion (Michael donor) conjugates to the α , β -unsaturated carbonyl (Michael acceptor) in the acrylate to form an intermediate anion, which obtains a hydrogen from the conjugate acid to form the final thioether product [14]. Poly(ethylene glycol) (PEG) is often the dominant precursor in hydrogels, since it is a biocompatible polymer and FDA approved for implantation *in vivo* [15].

Moon and colleagues used aqueous NaHCO₃ as the base catalyst to synthesize an injectable poly(ethylene glycol) diacrylate (PEGDA) based hydrogel with the three-arm, trithiol crosslinker ethoxylated trimethylolpropane tri-3-mercaptopropionate (Thiocure ETTMP) for use as a packing material during cancer brachytherapy [16]. The PEGDA molecular weight and acrylate: thiol stoichiometric ratios minimally influenced hydrogel properties. However, preliminary findings indicated NaHCO₃ concentration and water content tuned the hydrogel properties, although this was not systematically investigated. In a separate study, Khan and coworkers utilized a similar platform with NaOH catalysts to assess the impact of polymer concentrations and stoichiometric ratios [17]. While a slight excess of thiol was favorable and monomer concentrations modulated hydrogel properties, the researchers focused on optimizing their platform as a three-dimensional (3D) in vitro cancer cell culture model. Peach and colleagues [18] demonstrated the PEGDA-Thiocure hydrogel which utilizes NaHCO₃ conforms to anatomical structures in cadavers in situ and produces minimal heat upon crosslinking. In this study, we therefore selected this biomaterial platform and systematically varied across three levels the initial hydration level (25, 50, and 75 wt% water) and aqueous NaHCO₃ concentration (0.1, 0.175, 0.25 M) and characterized the 9 resulting formulations based on physical, biological, and chemical compatibility with the GBM microenvironment and our proposed application. We aimed to 1) identify and establish structure-property relationships between the hydration/basicity and hydrogel properties and 2) determine the most optimal formulation for compatibility with GBM therapy.

2. Materials and Methods

2.1 Hydrogel Synthesis

PEGDA with numbered average molecular weight of 575 g/mol (Sigma Aldrich) and Thiocure ETTMP 1300 333L (generously donated by Bruno Bock Thiochemicals) were brought to room temperature. Aqueous NaHCO₃ (Fisher Chemical) was prepared at 0.1 M, 0.175 M, and 0.25 M by dissolving appropriate masses in high performance liquid chromatography (HPLC) deionized (DI) water (Fisher Scientific). Hydrogels were prepared with a 1:1 stoichiometric ratio of thiol:acrylate with 0.300 g of PEGDA and 0.389 g of Thiocure. A volume of 0.230, 0.690, and 2.050 mL of NaHCO_{3(aq)} was used to prepare 25, 50, and 75 wt% water content hydrogels, respectively. PEGDA was dissolved in the appropriate volume of NaHCO_{3(aq)} by vortexing for 10 seconds, and Thiocure was injected into this solution and mixed vigorously with a stir rod for 20 seconds. Hydrogels were crosslinked in 6 dram vials (Fisher Scientific) at 37°C. Three replicates were synthesized for each of the 9 hydrogel formulations at the three varying hydration levels and NaHCO₃ concentrations to quantify the gelation times. Completion of reactions was verified in vials with the inversion method.

2.2 Swelling Studies

Hydrogels were prepared according to section 2.1. The mass was recorded for each as prepared hydrogel (m_d), after which point the hydrogel was submerged in 50 mL of 1X phosphate buffered saline solution (PBS) (Gibco) pre-equilibrated to 37°C in a jar. Hydrogels were maintained at 37°C and at 10-minute intervals for 3 hours, the hydrogel was taken out of the PBS, patted dry with Kimwipe, measured with a scale to quantify the wet mass (m_w), and

placed back in PBS. The swelling ratios were determined based on the percent mass increase in the hydrogels due to PBS absorption according to Equation [1] as follows:

Percent mass increase =
$$\frac{m_w - m_d}{m_d} \times 100$$
 [1]

Hydrogels were monitored daily to obtain the swelling ratios at equilibrium as well as the time point at which equilibrium was achieved.

2.3 Rheology

Three replicates of hydrogels per formulation were synthesized to possess 2 mm thicknesses and were excised to 10 mm x 10 mm dimensions. These hydrogels were swelled and maintained in 10 mL of 1X PBS at 37°C for 12 hours prior to rheological analysis. Each hydrogel was placed on a 25 mm plate in an RSA-G2 solids analyzer (TA Instruments), which was a linear rheometer that subjected the hydrogel to compression at 37°C. The gap between plates was less than 2.5 mm to maintain a force of 0 N. A frequency sweep from 0.1 to 10 Hz was performed at 2% strain in the linear viscoelastic region to collect the values for the storage and loss moduli (TA Trios). The final data are reported at 1 Hz during plateau.

2.4 Mesh Size

The hydrogel mesh size is the distance between crosslinks and impacts loading capacities and release profiles of encapsulated agents [19]. Since hydrogel viscoelastic properties impact the microstructure, the rheological data were used to calculate average mesh sizes (η) according to the rubber elastic theory [19], as indicated by Equation [2]. N_A is Avogadro's number, R is the universal gas constant (J mol⁻¹ K⁻¹), T is temperature (K), and G' is storage modulus in Pa as follows:

$$\eta = \sqrt[3]{\frac{G'N_A}{RT}}$$
 [2]

The crosslinking density (ζ) indicates the number of elastically active junctions in the network per volume and was determined from the rubber elastic theory according to Equation [3], where G_e is the storage modulus value at plateau during a frequency sweep [20].

$$\zeta = \frac{G_e}{RT}$$
 [3]

2.5 Gel Fraction

A 12 well plate was used as a mold to prepare 1 mL volume hydrogels. Three replicates were prepared for each formulation. Hydrogels were transferred to a watch glass and the masses were recorded. Hydrogels were air dried for 24 hours and then dried *in vacuo* for 48 hours or more at room temperature until fully dry. Dried masses were recorded (m_{dry}), and dried hydrogels were incubated in 25 mL of dichloromethane (Millipore Sigma) in a jar and placed in a mini shaker (Fisher Scientific) at room temperature with speeds of 150 rpm for 24 hours to extract soluble components. Hydrogels were transferred to a watch glass and air dried at room temperature for 24 hours and then dried *in vacuo* for 48 hours or more until completely dry. The final extracted and dried hydrogel masses were recorded (m_{ex}). The percentage gel fraction can be determined using Equation [4] as follows:

Gel Fraction (%) =
$$\frac{m_{ex}}{m_{dry}} \times 100$$
 [4]

2.6 Degradation

1 mL volume hydrogels were prepared in 9.5 dram vials with three replicates for every formulation at each time point: days 0, 3, 6, 9, 12, and 15 for total 18 hydrogels. Day 0 hydrogels were placed in a watch glass and air dried for 24 hours and then dried *in vacuo* for 48 hours or more at room temperature until completely dry. Final dried masses were recorded (m₀). The remaining hydrogels were submerged in separate vials containing 14 mL of 1X PBS with magnesium and calcium (Fisher Scientific) and placed in the incubating mini shaker with a speed

of 150 rpm at 37°C. At the designated time point, relevant hydrogels were taken out from the vials, washed three times with 10 mL of HPLC DI water to remove residual salt from the surface [21], and placed in a watch glass to air dry for 24 hours and then dry *in vacuo* for 48 hours or more until completely dry at room temperature. The final dried mass for each time point was recorded (m_f). PBS was refreshed completely every three days. The degradation at each time point was calculated as the percent mass loss with respect to the dried hydrogels at day 0 according to Equation [5]:

Percent mass loss =
$$\frac{m_0 - m_f}{m_0} \times 100$$
 [5]

2.7 Cell Culture and Preparation of Sterile Hydrogels

Normal Human Astrocytes (NHA) from Lonza were cultured in Astrocyte Growth Medium (AGM) from Lonza containing fetal bovine serum, L-glutamine, recombinant human epidermal growth factor, ascorbic acid, gentamicin sulfate amphotericin B, and insulin. The cells were maintained in T-25 flasks at 37°C and 5% CO₂ and passaged upon reaching 80% confluence according to the manufacturer's protocol. Cells from passages 5 - 7 were used for all experiments. Sterile hydrogels were prepared inside a biosafety cabinet under aseptic conditions with autoclaved dram vials and UV radiation sterilized equipment. Autoclaved HPLC DI water was used to dissolve NaHCO₃. Aqueous NaHCO₃, PEGDA, and Thiocure were all sterile filtered through 0.22 μm filter units (Millex). 500 μL volumes of hydrogels were synthesized and dispensed into 24 well plate molds and crosslinked in the incubator at 37°C. Each hydrogel was submerged in 1 mL of AGM for 24 hours to pre-equilibrate prior to seeding cells.

2.8 Cytotoxicity

The pH of the media after hydrogels reached equilibrium was recorded with a pH meter (Accumet Basic). The alamarBlue (AB) assay (BioRad) was used to quantify potential cytotoxicity of hydrogels to NHA by monitoring proliferation of cells cultured on hydrogel

surface according to the manufacturer's protocol. Pre-equilibrated media in hydrogels was discarded and 50,000 NHA were seeded on each hydrogel's surface. Four replicates of hydrogels were synthesized for each time point at each formulation and wells were filled with 1.5 mL AGM. A positive control for the assay was conducted with 50,000 NHA seeded directly on the surface of each tissue culture treated well (n = 4) to assess cell proliferation under standard cell culture conditions. The alamarBlue incubations were performed for 4 hours at the designated time point (day 1, 3, 5, and 7) with media containing 10% AB reagent by volume. Media with AB reagent only and no cells was used as negative controls. Spectrophotometer (SpectraMax M2^e Molecular Devices) absorbance readings were conducted for each sample with 3 subsamples at 570 nm and 600 nm. Cell density data for a standard curve relating the spectrophotometer absorbance to the astrocyte cell concentrations on well plates ranging from 1000 – 100,000 cells was also conducted with the same procedure. The standard curve data was curve fitted and the resulting equation was used to transform the absorbances from the experimental samples to a cell density as the cells proliferated. The astrocyte proliferations reported for the cytotoxicity assay are the final cell densities at each time point on the hydrogel or positive control sample normalized to the initial cell seeding density for each sample (50,000) NHA).

2.9 Immunoassay

An Enzyme-Linked Immunosorbent Assay (ELISA) was used to quantify the interleukin 6 (IL-6) secretion from NHA seeded on the hydrogels. Sterile hydrogels were synthesized in 24 well plate molds and pre-equilibrated with 2 mL of AGM at 37°C for 24 hours. 50,000 NHA were seeded and cultured on each hydrogel surface or directly on the tissue culture treated 24 well plate in triplicate at 37°C and 5% CO₂. All samples were refreshed with 2 mL of AGM every other day. At designated time points (days 1, 3, 5, 7, 9, 11, 13, and 15), the media was

collected and centrifuged at 1500 rpm for 10 minutes at room temperature. 1.5 mL of the supernatant was collected and stored at -80°C until use. A scratch wound was performed on NHA cultured directly on the wells after collecting the supernatant on day 5, when NHA reached 100% and complete confluency as outlined by a previously established protocol [22]. Briefly, the scratch wound was applied by dragging a sterile 200 µL pipette tip as a single line across the diameter of the well. Detached cells were removed by washing the well thrice with 1 mL of PBS and then replenishing the media. This scratch wound was used as a positive control for the immunoassay to compare IL-6 secretions of NHA exposed to hydrogels with IL-6 secretions from reactive astrocytes. Frozen supernatants were brought to room temperature and Human IL-6 DuoSet ELISA kit (R&D Systems) was used to quantify IL-6 concentrations in the 1.5 mL of supernatant according to the manufacturer's protocol. Spectrophotometer readings were taken at 450 nm with reference readings at 570 nm to account for wavelength corrections. The 4P logistic sigmoid curve fit (JMP) was used to model the standards and obtain the IL-6 secretion concentrations from the absorbances.

2.10 Immunocytochemistry

The glial fibrillary acidic protein (GFAP) intensity and morphology of NHA cultured on hydrogels were monitored with confocal microscope imaging. Hydrogels were synthesized in polydimethylsiloxane (PDMS) mold cutouts that were 10 mm in diameter and 1 mm in depth according to a previous protocol [23]. Each stamp was autoclaved, plasma treated (Harrick Plasma) for 4 minutes, and sterilized by UV radiation for 30 minutes. The stamps were incubated with sterile 1% polyethylenimine for 10 minutes, sterile 0.1% glutaraldehyde for 20 min, and washed with sterile DI water. Each stamp was placed in 24 well plate wells, and 90 μL volumes of sterile hydrogel precursors were dispensed into the stamp and crosslinked at 37°C for 30 minutes, followed by equilibration with 1 mL of AGM for 24 hours at 37°C prior to cell seeding.

For the positive control, a custom 3D printed polylactic acid (PLA) plate with 14 mm diameter and 12 mm deep wells was fitted with No. 1.5 thick 18 mm x 18 mm glass coverslips on the bottom (Fisher Scientific) for imaging cells. These plates were plasma treated, followed by 70% ethanol treatment and UV sterilization. The coverslips were coated with 2% gelatin solution according to the manufacturer's protocol (Sigma Aldrich) and thereby enable NHA adherence on the glass coverslip to image the cells as a control for standard cell culture cultivation on surfaces.

Samples were stained and imaged on days 1, 3, 5, 7, 9, 11, 13, and 15 for each formulation and control sample. All incubations were performed at room temperature in the dark unless otherwise noted. Washing steps were performed thrice with 1X PBS. For each time point, three PDMS-hydrogel composites were prepared for every formulation and three samples were prepared for the control condition on glass coverslips. 20,000 NHA were seeded on glass coverslip wells, while 100,000 NHA were seeded on the hydrogel surface. All samples were cultured in 1 mL of AGM, refreshed every other day, and maintained at 37°C and 5% CO₂. At designated time points, media was removed and samples were washed, then fixed with 10% formalin (Sigma Aldrich) for 20 minutes. After washing, samples were permeabilized with 0.5% TritonX-100 (Polysciences, Inc) for 20 minutes, washed, and blocked with 1% bovine serum albumin (BSA) (Fisher Bioreagents) for 1 hour. After washing, samples were incubated with GFAP monoclonal antibody GA5 (Life Technologies) (1:200) overnight at 4°C. Samples were washed and incubated with goat anti-mouse IgG1 cross-adsorbed secondary antibody Alexa Fluor 488 (Life Technologies) (1:1000) for 1 hour. After washing, samples were counterstained with 0.1 μg/mL DAPI (Sigma Aldrich) for 30 minutes (hydrogels) and 10 minutes (control). The cells were washed prior to imaging with an EC Plan-Neofluar 40X objective lens with a numerical aperture of 0.75 in a Zeiss LSM 800, axio observer Z1/7 inverted confocal microscope to obtain morphology and GFAP intensity of the astrocytes. Z-stacks with 300 µm thickness were used to confirm the cells had not invaded into the hydrogel and had remained on the surface. PDMS-hydrogels were carefully removed from the well and inverted onto a No 1.5 glass coverslip coated with a 20 µL droplet of PBS for imaging the astrocyte monolayer on the hydrogel surface. Control conditions were imaged directly from the glass coverslip on the bottom of 3D printed well plates. Three fields of view were randomly selected per hydrogel or well plate, and all images were taken with a 45 µm size pinhole and 8x averaging. All acquired images were 1.85 µm thick optical sections of the astrocyte monolayer focused on the hydrogel surface or gelatin coated glass coverslip. These optical section images were analyzed and processed with Zen 3.3 software (Zeiss Zen Lite). The normalized GFAP fluorescence intensity was determined in a semi-quantitative manner for the astrocytes cultured on the hydrogel surface. This value was determined based on the ratio of the average fluorescence intensity per pixel for each individual cell to the average fluorescence intensity in the background for the field of view containing the same cell to account for changes in microscope setup over time, according to previous protocols [24, 25]. Control samples without primary antibody were used to confirm the lack of non-specific binding of the secondary antibody to NHA or the hydrogel.

2.11 Statistical Methods

Quantitative data are represented as means \pm standard deviations. All experiments were conducted in triplicate or more. Tukey's post-hoc test (JMP) for multiple pair-wise comparisons was performed using one way ANOVA, with p-values < 0.05 considered statistically significant.

3. Results

3.1 Hydrogel Synthesis

Hydrogels were synthesized with PEGDA and Thiocure precursors with NaHCO_{3(aq)} and crosslinked at 37°C, as illustrated by the schematic in Figure 1. According to Table 1, increasing

NaHCO₃ concentrations generally decreased gelation times. This trend was apparent in hydrogels with 25 wt% water, but this trend was not observed in 75 wt% hydrogels. Hydrogels with 0.1 M NaHCO₃ and 25 wt% hydration had the highest gelation time at 856 ± 20 s, while hydrogels with 0.25 M and 50 wt% had the lowest gelation time at 14 ± 1 s.

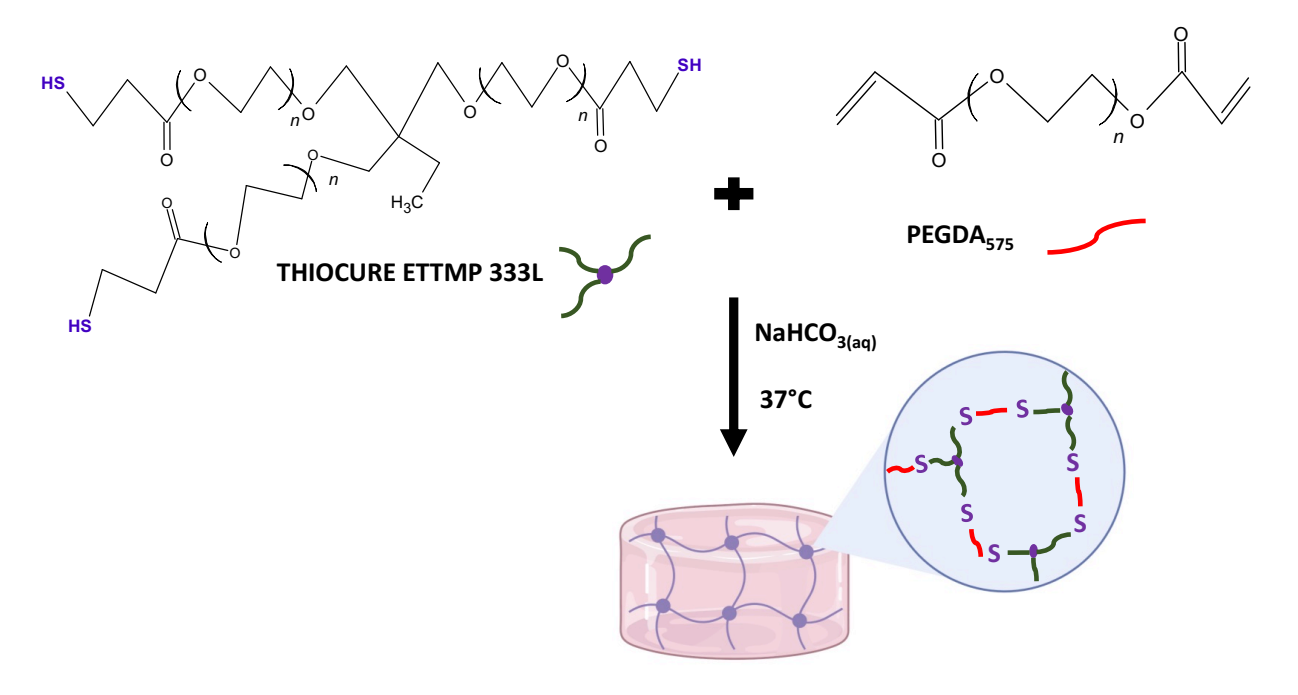


Fig. 1. Schematic representation of the synthesis method for generating the thiol-Michael addition hydrogels. PEGDA and Thiocure precursors were crosslinked in a 1:1 stoichiometric ratio by NaHCO_{3(aq)} base catalysis at physiologic temperature. Created with BioRender.com and ChemSketch.

Table 1. Gelation time and time to reach equilibrium swelling for hydrogel formulations.

Water Content (%)	NaHCO ₃ Concentration (M)	Average Gelation Time (s)	Time to Reach Equilibrium Swelling (h)
	0.1	856 ± 20	77.500
25	0.175	46 ± 1	2.500
	0.25	21 ± 1	3.000
	0.1	38 ± 1	3.000
50	0.175	41 ± 3	102.500
	0.25	14 ± 1	76.000
	0.1	36 ± 1	0.000
75	0.175	41 ± 1	0.167
	0.25	37 ± 2	0.167

3.2 Swelling Studies

Upon implanting a hydrogel in the brain, the diffusion of cerebrospinal fluid may cause it to swell. Hydrogels were therefore swelled in PBS and according to the swelling kinetics (Fig. 2A), all formulations swelled continuously for 180 minutes, except for hydrogels with 75 wt% water content. The 75 wt% hydrogels deswelled and exhibited the highest variations in swelling kinetics data. The 25 wt% hydrogels swelled the most with equilibrium ratios ranging from 0.66 to 0.77 (Figure 2B), while 50 wt% hydrogels swelled the least (0.25 – 0.31) with the lowest variation. The 0.175 M and 50 wt% hydrogel took the longest time to reach equilibrium swelling at 4 days (102.500 hours), while the remaining formulations reached equilibrium in 3 days or less (Table 1). All formulations were transparent while swelling, except for the 75 wt% hydrogels that became opaque during swelling in PBS at 37°C (Fig. 2C). The 75 wt% hydrogels were screened out from further study due to poor crosslinking.

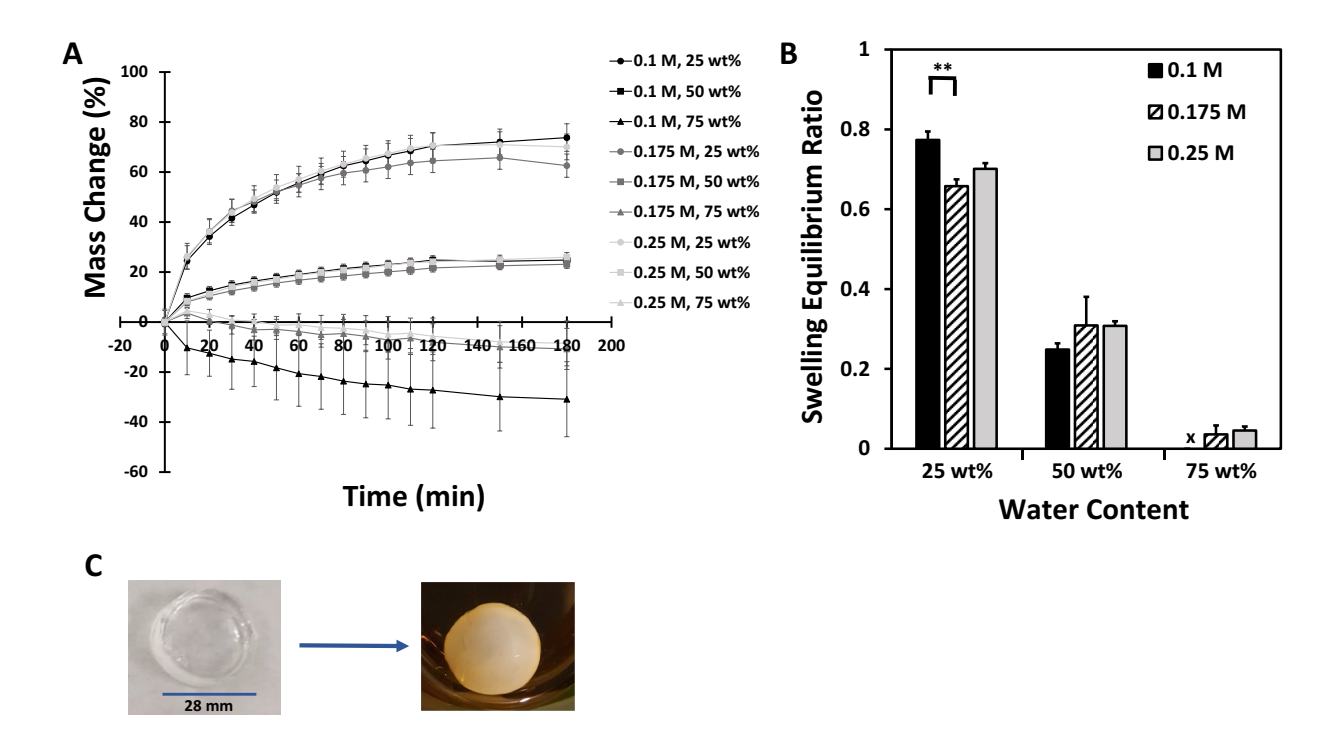


Fig. 2. Effect of hydration level and NaHCO₃ concentration on hydrogel swelling. Hydrogels were swelled in phosphate buffer saline solution (PBS) at 37°C. (A) Swelling kinetics obtained at 10-minute intervals for up to 180 minutes. (B) Swelling ratios at equilibrium. 0.1 M, 75 wt% hydrogel never reached equilibrium (x). ** p-value < 0.01, error bars represent standard deviations (n = 3). (C) Change in opacity for hydrogel formulation at 0.25 M NaHCO₃ and 75 wt% water content upon swelling at 37°C in PBS.

3.3 Rheology and Hydrogel Microstructure

According to the data in Figure 3A, the 0.25 M at 50 wt% formulation possessed the highest storage modulus (69.2 \pm 3.5 kPa). The other 5 formulations had storage moduli ranging from 3.9 – 25.5 kPa. There were no trends or significant differences in storage modulus among the 25 wt% hydrogels. In contrast, the storage modulus increased with increasing NaHCO₃ concentration for 50 wt% hydrogels, with a significant difference between 0.1 M and 0.25 M NaHCO₃. The tan δ values representing the ratio of the loss modulus (G'') to storage modulus (G') ranged from 0.10 to 0.36 for all formulations (Figure 3B). The hydrogel mesh sizes are summarized by Table 2. 25 wt% water content hydrogel mesh sizes were consistently around 8 nm, while the mesh sizes for 50 wt% hydrogels decreased with increasing base concentration and ranged from 4.2 – 11.0 nm. The crosslinking densities were inversely proportional to mesh sizes

and increased with base concentration in 50 wt% hydrogels, with no such trend in 25 wt% hydrogels. The 0.25 M, 50 wt% hydrogels possessed the highest crosslinking density at $26.9 \pm 14.3 \text{ mol/m}^3$.

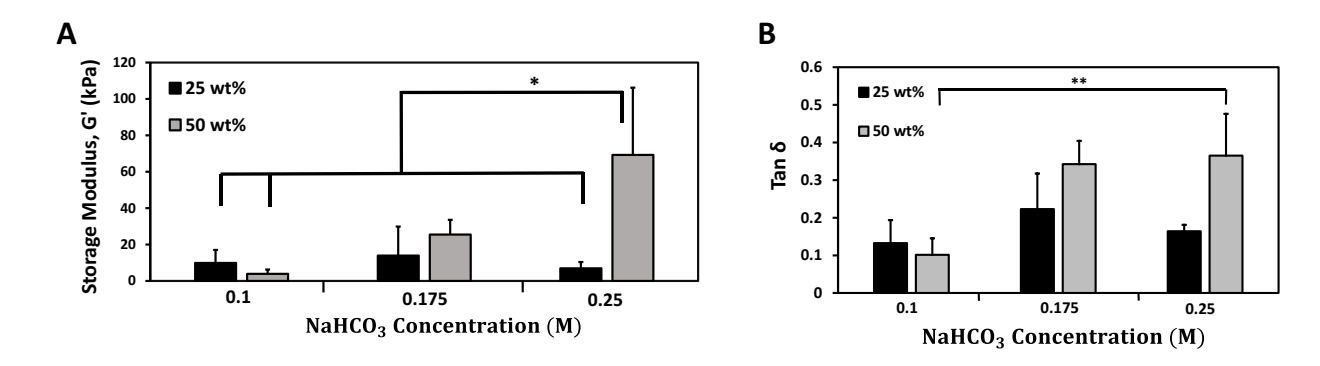


Fig. 3. Rheological analysis of hydrogel formulations. All hydrogels were swelled for 12 hours in PBS at 37°C before being subjected to the compression mode in an RSA-G2 at 2% shear strain and frequency sweep from 0.1 to 10 Hz at 37°C. Hydrogels with dimensions of 10 mm x 10 mm x 2.5 mm were used for each formulation. Data reported for 1 Hz at plateau. (A) Storage modulus. (B) Tan δ values for ratio of the loss modulus (G'') to the storage modulus (G'). * p-value < 0.05, ** p-value < 0.01, error bars represent standard deviations (n = 3).

Table 2. Hydrogel mesh sizes and crosslinking density based on rubber elastic theory.

Water Content (%)	NaHCO ₃ Concentration (M)	Average Mesh Size (nm)	Average Crosslinking Density (mol/m³)
25	0.1	8.4 ± 2.4	3.8 ± 2.8
	0.175	8.2 ± 2.8	5.4 ± 6.2
	0.25	8.8 ± 1.3	2.7 ± 1.4
50	0.1	11.0 ± 2.3	1.5 ± 0.9
	0.175	5.6 ± 0.6	9.9 ± 3.1
	0.25	4.2 ± 0.8	26.9 ± 14.3

3.4 Degradation

The fastest degradation was observed for 0.25 M and 50 wt% hydrogels, with approximately 5.9% loss in mass per day (Figure 4A) and a total of 92.9% loss in the original mass after 15 days (Figure 4B). For 50 wt% hydrogels, degradation increased with increasing NaHCO₃ concentration. In contrast, changes in base concentrations did not significantly impact the degradation of 25 wt% hydrogels. 25 wt% hydrogels had slow degradation rates after day 6, while degradation continued to increase for 50 wt% hydrogels at 0.25 M and 0.175 M. The 0.1

M and 25 wt% hydrogels had the lowest degradation rate at only 1.5% mass loss per day, with only 26.0% loss in its original mass after 15 days. As indicated by Figure 4C, this hydrogel formulation remained stable throughout the 15 days.

3.5 Gel Fraction

Although the gel fractions did not differ significantly across the different formulations, both 0.25 M hydrogels were below 80% gel fractions (dotted line) with a high standard deviation (Figure 4D) and were screened out from further study due to an insufficiently crosslinked polymer network. The 0.175 M hydrogels had the highest gel fractions at 90.9% and 85.2% for the 25 wt% and 50 wt% hydrogels, respectively, and possessed the lowest variations in the data.

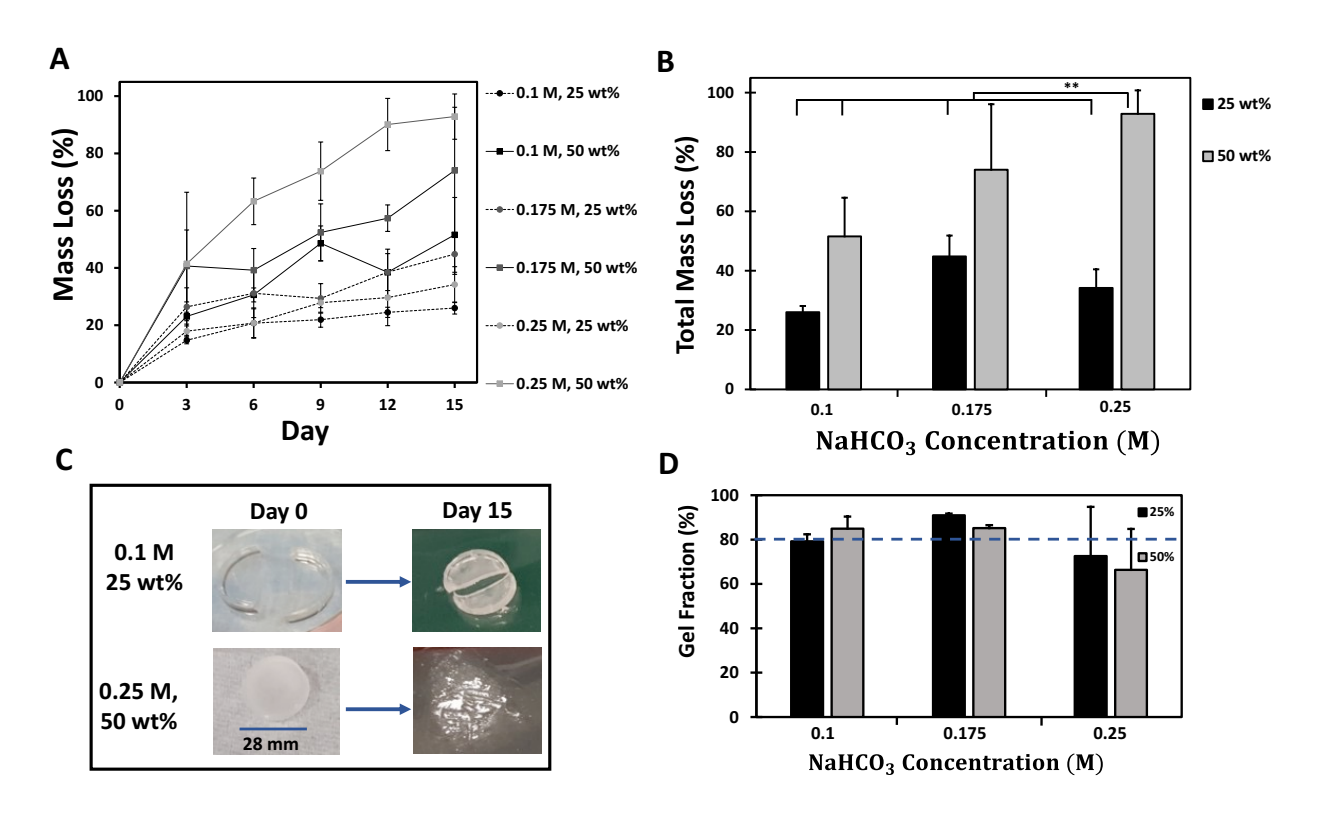


Fig. 4. Effect of NaHCO₃ concentration and hydration level on hydrogel stability. (A) Degradation kinetics profile of hydrogels over 15 days. (B) Total degradation of hydrogels after 15 days. Hydrogels were submerged in PBS at 37°C in triplicate. Degradation in terms of mass loss upon drying. (C) Comparison of hydrogels on Day 0, before degradation began, to Day 15. (D) Percent gel fraction and strength of polymer network. Soluble components of hydrogels were extracted with dichloromethane. Dashed line is 80% threshold. ** p-value < 0.01, error bars represent standard deviations (n = 3).

3.6 Cytotoxicity Assay

After 24 hours of equilibration, the pH of media that submerged the 25 wt% hydrogels at 0.1 M and 0.175 M NaHCO₃ was determined to be 6.2. For the 50 wt% hydrogels at 0.1 M and 0.175 M, the media pH was 6.9 and 7.1, respectively. NHA proliferations at each time point were determined by normalizing the final cell densities to the initial cell seeding densities and ranged from 78% to 153% during the 7-day period, as indicated by Figure 5A. During the first 24 hours, both 0.175 M hydrogels had significantly higher cell proliferations (120% – 125%) than the 0.1 M hydrogels (77% – 85%). By day 7, both 50 wt% hydrogels had significantly higher cell proliferations (142% – 153%) than 25 wt% hydrogels (114% – 115%) (Figure 5B). 0.175 M and 50 wt% hydrogels had the highest proliferations throughout the 7 days. NHA proliferations in the control condition with cells cultured directly on tissue culture treated wells increased from 305% on Day 1 during the first 24 hours of culture to 381% on Day 7. Both the 25 wt% hydrogels (0.1 M and 0.175 M) were screened out from further characterization due to significantly lower cell proliferations on day 7 compared to 50 wt% hydrogels.

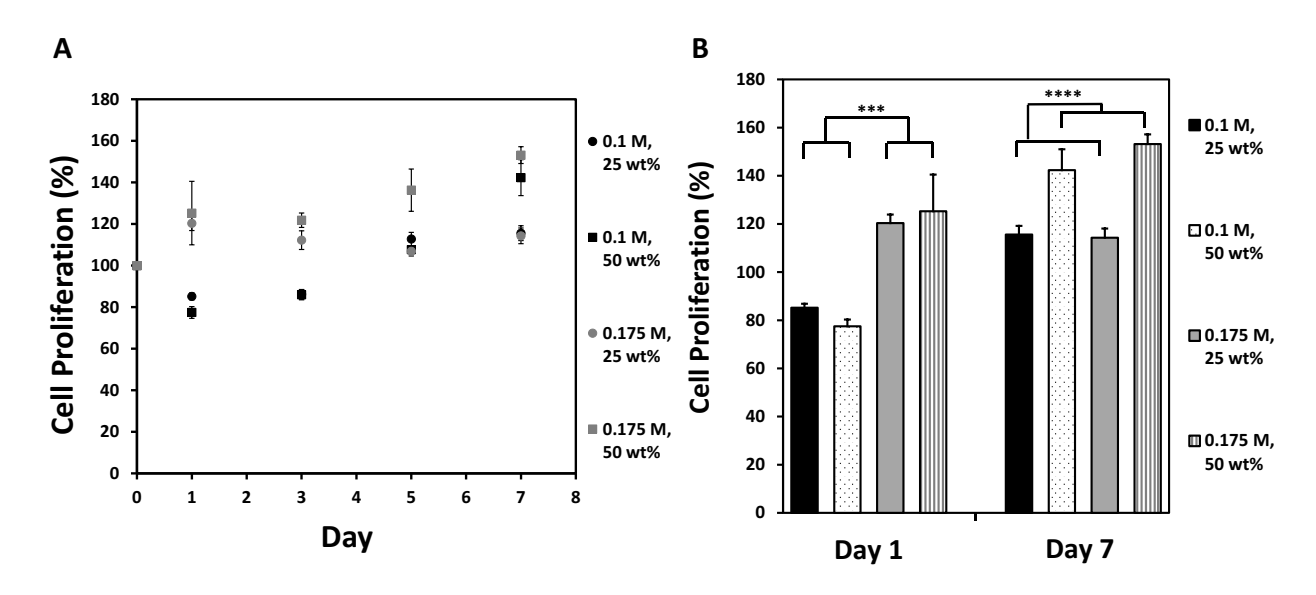


Fig. 5. Cytotoxicity of hydrogels to normal human astrocytes. (A) Cell proliferation (%) over 7 days for astrocytes cultured as a monolayer on hydrogel surface. (B) Cell proliferation (%) of astrocytes cultured as a monolayer on hydrogel surface on day 1 and day 7. Hydrogels were pre-equilibrated with media prior to cell culture. Astrocytes seeded at a density of 50,000 cells per hydrogel. Cell cultures maintained at 37°C with 5% CO_2 in astrocyte growth media. Cell proliferations quantified with alamarBlue assay and determined by normalizing the final cell densities at each time point to the initial cell seeding densities. *** p-value < 0.001, **** p-value < 0.0001, error bars represent standard deviations (n = 4).

3.7 Immunoassay

NHA cultured on hydrogels secreted IL-6 with concentrations from 23.5 pg/mL to 238.7 pg/mL in 1.5 mL of culture media supernatant (Figure 6A). The secretion profiles for the two formulations (0.175 M and 0.1 M at 50 wt%) were similar. IL-6 secretion profiles were also normalized to cell densities at each time point to directly compare IL-6 concentrations on a per cell basis up to day 7, before hydrogels began to degrade significantly, with results indicating secretion peaked on Day 5 for 0.175 M and on Day 7 for the 0.1 M hydrogels (Supplementary Figure S1). From Day 7 and onwards, IL-6 secretions began to decline for both formulations (Figure 6A). NHA cultured on well plates secreted significantly higher IL-6 than the hydrogels after the scratch wound was applied on Day 5 according to the normalized secretion profile (Supplementary Figure S1). The 7-day cumulative and normalized data (Figure 6B) demonstrated IL-6 secretion between the two formulations was not significantly different, with

0.0081 pg/cell and 0.0093 pg/cell for 0.175 M and 0.1 M hydrogels, respectively. In contrast, cumulative and normalized IL-6 secretions for wounded NHA were an order of magnitude higher at 0.0230 pg/cell.

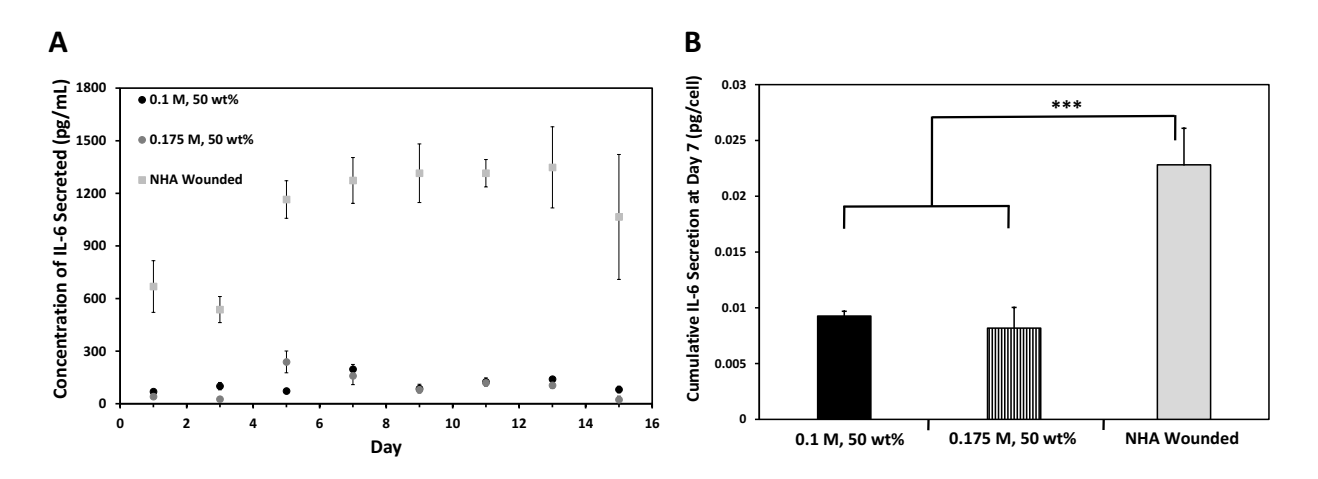


Fig. 6. Immunogenic response and IL-6 secretion of normal human astrocytes cultured on surface of the hydrogels. Astrocytes were seeded on the surface of hydrogels at a density of 50,000 cells per hydrogel or well plate and cultured for 15 days. Cell cultures maintained at 37°C with 5% CO₂ in astrocyte growth media. 1.5 mL culture media supernatants were collected and analyzed by ELISA to quantify IL-6 secretion. A scratch wound assay was performed on astrocytes seeded on the control well plate cell culture conditions on Day 5. (A) IL-6 secretion over 15 days. (B) Cumulative IL-6 secretion on Day 7 normalized to astrocyte cell density from each time point. *** p-value < 0.001, error bars represent standard deviations (n = 3).

3.8 Immunocytochemistry

1.85 μm thick optical sections of astrocytes as a monolayer on the surface of the hydrogels or on gelatin-coated glass coverslips (control) are indicated by the confocal microscope images in Figure 7A. NHA cultured on the hydrogels maintained a round morphology throughout 15 days, while cells elongated in the control condition. The average GFAP fluorescence intensities of astrocytes cultured on the hydrogels were normalized to the background fluorescence and these levels ranged from 18.2 to 65.6 on 0.175 M and 50 wt% hydrogels, with highest values from days 1 – 3 (Figure 7B). For cells cultured on 0.1 M and 50 wt% hydrogels, the normalized GFAP fluorescence intensity ranged from 22.5 – 88.3 and peaked on day 5, at which point it was significantly higher than days 7, 9, and 15 for 0.175 M hydrogels

and days 9, 13, and 15 for 0.1 M hydrogels. For both hydrogels, GFAP levels decreased and plateaued after reaching the highest values. NHA diameters ranged from 13.3 – 35.1 μm, peaking on day 3 for 0.1 M hydrogel, which was significantly higher from the NHA diameters for all 0.175 M hydrogels and NHA diameters from days 5 and onwards for 0.1 M formulations (Figure 7C). NHA average cell diameter and normalized GFAP fluorescence intensity had a weak positive association with a correlation of 0.23 (Figure 7D).

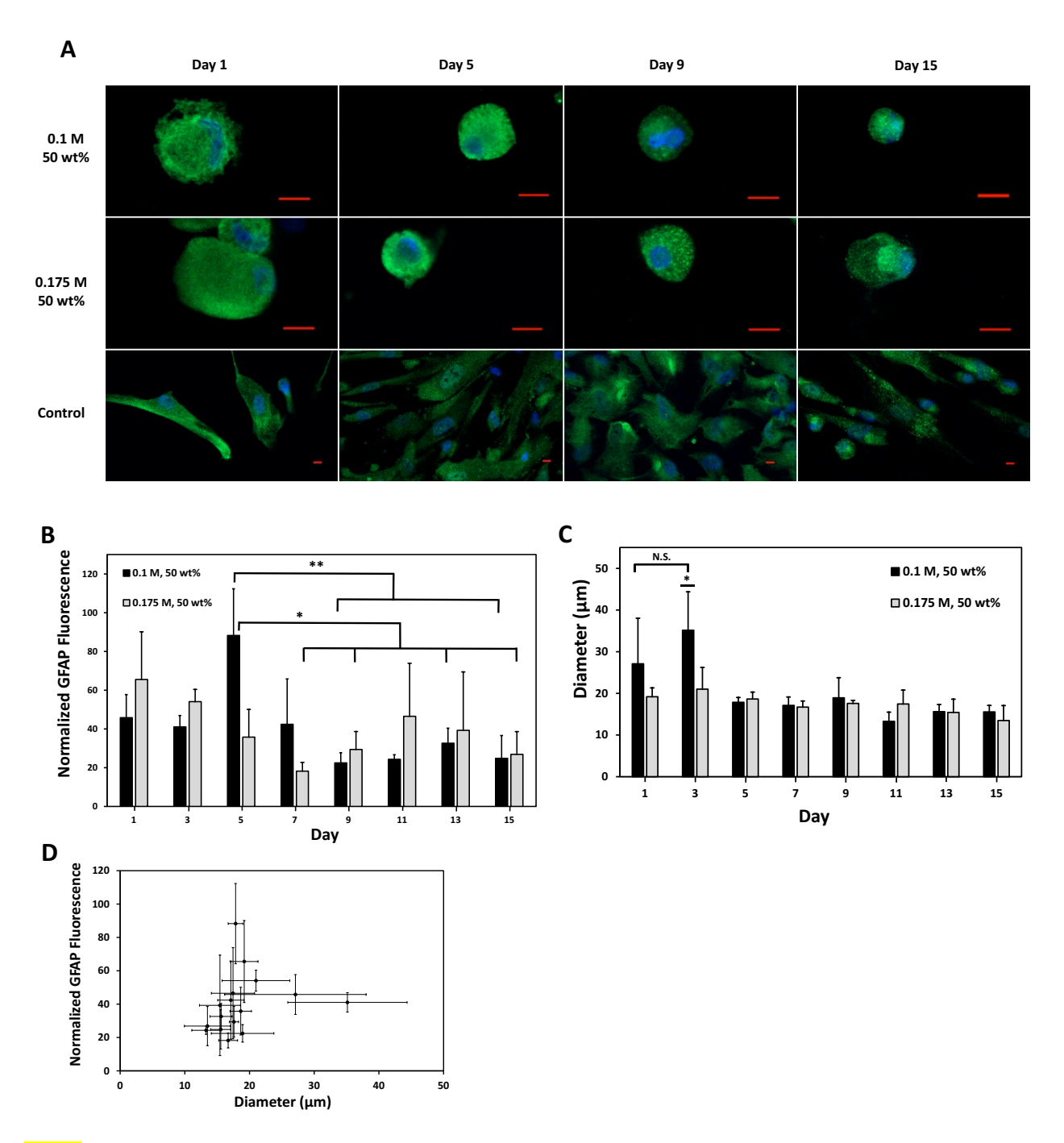


Fig. 7. Normal human astrocyte reactivity to hydrogels. Astrocytes were seeded on surface of hydrogels at a density of 100,000 cells per hydrogel and 20,000 cells per well under control cell culture conditions. Cell cultures were maintained at 37° C in 5% CO₂ and imaged with confocal microscopy every other day for 15 days. All acquired images are $1.85 \mu m$ thick optical sections focused on the astrocyte monolayer on hydrogel surface or well plate. (A) Morphology of astrocytes. Green stain is GFAP, blue stain is DAPI. Scale bar is $10 \mu m$. (B) Normalized GFAP fluorescence intensity of astrocytes on hydrogels. (C) Average diameters of astrocytes on hydrogels. (D) Correlation between normalized GFAP fluorescence intensity and cell diameter of astrocytes on hydrogels had a value of 0.23. * p-value < 0.05, ** p-value < 0.01, error bars represent standard deviations (N = 3, n = 3).

4. Discussion

This study aimed to develop an injectable thiol-Michael addition hydrogel that is physically, chemically, and biologically compatible with the GBM microenvironment. Nine different formulations were generated by tuning the initial water content and aqueous NaHCO₃ catalyst concentration, and these hydrogels were characterized to determine structure-property relationships and the most optimal formulation for GBM therapy. Except for the 0.1 M and 25 wt% hydrogels, all other formulations crosslinked rapidly. The 0.25 M hydrogels with 50 wt% and 25 wt% water content crosslinked within 14 – 21 seconds, which may be too fast for dispensing the hydrogel precursor solution in situ. In contrast, hydrogel formulations with 0.175 M crosslinked from 41 - 46 seconds, indicating their suitability as an injectable material for undergoing gelation within a clinically relevant timeframe [26] in the GBM resection cavity. Higher base concentrations generally decreased gelation times due to their role as catalysts in the reaction. However, varying the base concentrations did not impact 75 wt% hydrogels, since the high water content affected the kinetics of crosslinking. The longest gelation time was over 14 minutes for 0.1 M and 25 wt% hydrogels. Its low hydration led to rapidly increasing viscosity as crosslinking occurred, which likely decreased chain mobility, hindered crosslinking, and decreased the reaction rates [27]. The NaHCO₃ content during synthesis was also the lowest for this formulation due to the combined low water content and base concentration, and therefore the hydrogel took longer to crosslink.

Hydrogels thermodynamically interact with aqueous media in a manner similar to the extracellular matrix (ECM), which is why characterizing their swelling behavior is critical [21]. Excessive swelling can damage adjacent neurons, compromise patient safety, and decrease hydrogel functionality *in vivo* [21, 28]. The hydrogel swelling studies were conducted in 1X PBS to mimic artificial cerebrospinal fluid and physiologic pH and ionic strength. According to Roy

and Gupta [29], hydrogel swelling is primarily influenced by the pH, temperature, and analyte composition in the fluid. PBS and artificial cerebrospinal fluid are buffer systems comprising similar components such as sodium chloride, potassium chloride, potassium phosphate, and disodium phosphate. Furthermore, Baldwin and colleagues had found no significant differences in the response of an electrophysiological-thermal flow sensor between 1X PBS and artificial cerebrospinal fluid [30].

The initial water content overall had a greater impact on swelling behavior than NaHCO₃ concentrations, as a decrease in hydration increased swelling. All three 75 wt% hydrogels possessed a water content above equilibrium, and these formulations therefore deswelled over time. Swelling data can help identify hydrogels with batch-to-batch variations [31], and these three formulations also possessed the largest standard deviations (Figure 2A). The large variation in swelling behavior, the tendency to deswell, and the change in hydrogel opacity when submerged in PBS (Figure 2C) indicated the 75 wt% hydrogels were poorly crosslinked. The high hydration increased the base content during the synthesis, which lowered the hydrogel cloud point and led to a separation of phases. Pritchard and colleagues had also observed poor polymerization in hydrogels with increased salinity due to a lower cloud point [21]. 75 wt% hydrogels were therefore deemed unsuitable as chronic implants for GBM treatment and screened out from further characterization. In contrast, 50 wt% hydrogels exhibited the least batch-to-batch variability and lowest levels of swelling. The 25 wt% hydrogels swelled the most, since the initial water content was below the equilibrium swelling point. The 0.175 M hydrogel at 50 wt% took the longest time to reach equilibrium, which can be beneficial for GBM treatment by enabling adjacent neural tissues to gradually adjust to an expanding hydrogel in the resection bed.

The elastic modulus of normal brain tissue typically varies among patients with a value around 1 kPa [32]. Since the hydrogel storage moduli were all higher, the formulations can maintain structural integrity against distending tissue forces upon implantation. However, growing brain tumors are restricted to a confined skull space, which increases the pressure in vivo. Compression stiffening also increases due to fluctuations in ion conductance and a rise in GBM vascularization [33]. Furthermore, GBM tumorigenesis leads to ECM remodeling and an increase in rigidity, as high-grade glioma cells secrete 20 times more ECM components like hyaluronan compared to healthy brain cells to promote more migration and invasion along these denser and structured matrices [34]. Rheological analysis in compression mode was hence performed to mimic GBM compression stiffening. The storage modulus of GBM cells are typically between 0.1 – 10 kPa, while the upper limit can be as high as 50 kPa [35]. In their study, Wang and colleagues report that the stiffness of GBM tissues is around 25 kPa [36]. As is evident from Figure 3A, the storage modulus of the 0.25 M and 50 wt% hydrogel was above this threshold and may risk mechanical mismatch with soft brain tissue and the GBM microenvironment to augment an inflammatory response and patient discomfort. In contrast, the storage moduli of the other 5 formulations corresponded to GBM compression stiffening. Overall, the storage moduli of the 25 wt% hydrogels were lower than their 50 wt% counterparts, since the 25 wt% hydrogels swelled more with PBS prior to compression (Figure 2B). For 50 wt% hydrogels, the storage modulus and crosslinking density increased with base concentration, while there was no such clear trend for 25 wt% hydrogels. The low water content in 25 wt% hydrogels led to high viscosities, which likely dominated the matrix modulus and kinetics of crosslinking.

Tan δ values assess the viscoelasticity of a material [19]. Since all tan δ values were between 0 - 1, the storage moduli were higher than the loss moduli, indicating the hydrogels exhibited mostly elastic behavior [17]. This elasticity is beneficial to potentially capture GBM cells, since high loss moduli hinder cell movement in hydrogels by limiting material deformation in response to cell migration and motility [37]. Hence, stiff hydrogels with solid-like properties do not allow long polymer chains to rearrange [38] and thereby cells to infiltrate inside. On the other hand, GBM cell invasion into the hydrogel can potentially increase the pressure inside the material. Therefore, future work will need to characterize the hydrogel viscoelastic properties further when GBM cells are entrapped inside and determine to what extent the storage modulus increases.

The tight range in tan δ values and mesh sizes indicated hydrogels possessed homogeneous mechanical properties and microstructures. The rubber elastic theory was applicable for measuring the mesh sizes, since all formulations were elastic and can recover from small deformations [39]. As expected, higher crosslinking densities resulted in lower mesh sizes. The high storage modulus of 0.25 M and 50 wt% hydrogels can be attributed to its high crosslinking density, and its small mesh size may make it difficult to entrap GBM cells. 0.175 M and 50 wt% hydrogels with a 25.5 kPa storage modulus can conform to the GBM environment and withstand pressure from the elevated intracranial pressures. Its storage modulus is also suitable for a heterogeneous population of GBM cells, whether they prefer a high elastic modulus and are stiff-sensitive for migration and adhesion or are stiffness independent [40].

Degradation was conducted by submerging hydrogels in 14 mL of PBS, since resected GBM tumors are typically 3 cm in diameter and 14 mL of cerebrospinal fluid refill resected cavities [41]. A higher hydrogel hydration increased degradation, indicating that bulk erosion

and the hydrolysis of acrylate ester bonds in the hydrophilic PEGDA backbone were the dominant mechanisms for degradation [14]. Furthermore, the degradation profile (Figure 4B) aligned with the storage modulus data (Figure 3A). O'Shea and colleagues reported that increasing mechanical loads increase hydrogel degradation rates [42], and degradation profiles relate to hydrogel behavior under mechanical stresses. Interestingly, the degradation results also aligned with the crosslinking densities, as higher crosslink densities increased degradation.

Metters and Hubbel found crosslinking densities did not impact the degradation of their PEG-acrylate Michael-type hydrogels [43]. However, our results seem to indicate that for these PEGDA-Thiocure hydrogels, the onset of degradation in more densely packed crosslinks results in a cascade effect by promoting the degradation of more bonds in the same space.

A biodegradable hydrogel in the resection cavity is advantageous as an adjuvant therapy to conventional GBM treatments. For example, it can be used for therapeutic applications prior to degradation during the GBM post-wound healing process after surgical resection, when most patients wait less than 6 weeks before chemoradiotherapy [44, 45]. However, one potential limitation is that the hydrogel degradation rate can impact its cell entrapment capacity and ability to sustain the release of payloads. As such, the degradation profiles from Figure 4A can be used as a guide to tune the hydrogel degradation parameters to suit specific therapeutic GBM applications. In particular, it would be prudent to conduct further studies in the future to determine how long the hydrogel can retain cells or therapeutic payloads before significant degradation.

Another important consideration for biodegradable hydrogels in therapeutic glioblastoma applications is whether the degradation products are able to pass through the blood-brain-barrier. The blood-brain-barrier permeability enables the passage of small, lipophilic, positively charged

molecules between 400 – 600 Da [46]. Considering that the molecular weight of Thiocure is 1300 Da, its degradation products may not naturally pass through the blood-brain-barrier. Several technologies such as focused ultrasound [47] and high frequency electroporation [48] can temporarily disrupt the blood-brain-barrier for passage of drugs to treat intracranial tumors. Since our proposed hydrogel-based GBM treatment is compatible with these emerging technologies, the hydrogel biodegradation products will be able to pass through when the blood-brain-barrier is temporarily disrupted and opened. As such, it will be important to investigate in future research whether the hydrogel degradation products are naturally able to pass through the blood-brain-barrier or only when its permeability is enhanced.

The gel fraction data indicated that tuning the hydration and NaHCO₃ concentration did not significantly impact the strength of the polymer networks. Showalter and colleagues report catalyst efficiencies and temperatures have a larger impact on gel fractions [49]. Regardless, both 0.25 M hydrogels had gel fractions below 80%, which is a threshold for sufficient conversions and well crosslinked networks [49]. The low gel fractions in 0.25 M hydrogels can therefore risk leaching soluble components into the surrounding tissue and increasing the material cytotoxicity. Furthermore, the high variation in these 0.25 M gel fractions suggests a reduced homogeneity in the polymer network. The low gel fractions and high variations in the two 0.25 M formulations can be attributed to their very rapid gelation times of 14 – 21 seconds (Table 1), which may not have enabled the hydrogels to crosslink sufficiently. Coupled with a high storage modulus and degradation rate for 0.25 M and 50 wt% hydrogels, both 0.25 M hydrogels were therefore screened out from further study.

Astrocytes are the most abundant cell type in the glioma environment and most likely to interact with hydrogels, since neurons are typically displaced during implantation of neural

devices [50]. The cytotoxicity assay revealed the hydrogels were biocompatible with NHA. This biocompatibility aligns with previous studies that evaluated the cytotoxicity to healthy cells such as RAW-blue macrophage cells [42] and vaginal epithelial cells [16], which were all demonstrated to be highly viable against a similar thiol-acrylate hydrogel platform. The proliferation of astrocytes cultured on the hydrogel surface was monitored for up to 7 days, before the onset of significant hydrogel degradation (Figure 4A). As expected, the positive control yielded a significantly higher cell growth and faster proliferation rate than astrocytes cultured on the hydrogels, since the well plates were tissue culture treated and the surfaces were optimized for cell attachment and proliferation. According to Figure 5B, hydrogels with a higher NaHCO₃ concentration yielded higher cell proliferations during the first 24 hours and are better suited as acute implants, while a higher hydration level was favorable in the long term at day 7 for chronic implants. The two 0.175 M hydrogels yielded higher cell growth than the two 0.1 M hydrogels during the first 24 hours due to the higher crosslinking densities. Wilts and colleagues had demonstrated poly(lactic-co-glycolic-acid)-diacrylate hydrogels with lower crosslinking densities increased cytotoxicity for breast cancer epithelial cells due to the presence of free acrylate groups from a low conversion [51]. Hence, the high crosslinking density in the 0.175 M hydrogels likely reduced the number of free acrylate groups available and increased biocompatibility to NHA. The presence of free acrylates decreased over time and the hydration level dominated cell proliferations by day 7. The pH of 50 wt% hydrogels were closer to physiologic pH than 25 wt% hydrogels. The 25 wt% hydrogels were more acidic due to the lower NaHCO₃ content that was available to neutralize the acidic thiol and acrylate groups. Kasymov and colleagues report that astrocytes near or residing on the ventral surface of brain stems are highly sensitive to pH [52], so NHA thrived more on 50 wt% hydrogels in the long

term. 0.175 M and 50 wt% hydrogels were the most ideal for NHA proliferation due to the combined high water and base content, which resulted in the highest continuous proliferations above 100% throughout the 7 days. Since 50 wt% hydrogels had better cytocompatibility as a chronic implant and are better suited for GBM treatment, the two 25 wt% hydrogels were screened out from further study. The *in vitro* cytotoxicity assay was limited to 7 days to delineate cell proliferations on the hydrogel surface from proliferations on the tissue culture treated surface of the well plate upon hydrogel degradation. Future biocompatibility research with *in vivo* animal models can potentially explore the impact of the degradation products and their cytotoxicity to healthy brain cells for beyond 7 days.

Biomaterial implants can trigger an immune response, but the post-surgery reverse migration theory postulates an immune response can enhance GSC migration into the resection cavity [53]. When astrocytes become reactive due to an insult in the brain, they undergo morphological, cellular, and functional changes and secrete specific cytokines [54]. Reactive astrocytes release elevated levels of IL-6, thereby activating MMP-2 expression and upregulating fascin-1, an actin-bundling protein that helps cells form protrusions [55]. As a result, IL-6 promotes invasion and migration in GBM cells, including CD133+ GSCs [56] by remodeling the ECM [54]. The low levels of IL-6 secretion compared to the reactive astrocytes from the scratch wound indicated the hydrogels did not induce a significant inflammatory response. Since this secretion decreased with time, the astrocyte reactivity dwindled as NHA adapted to the hydrogel environment. Glial responses in the brain are constrained to a 50 micron radius around hydrogel implants, since the inflammatory factors are secreted by cells which directly contact the surface and therefore do not diffuse far before clearance from tissues [57]. IL-6 increases GBM migration and invasion, and this low secretion may help sensitize GBM/GSCs near the resection

cavity to migrate toward the injectable hydrogel in the resection cavity in response to the chemical gradient.

The normalized, cumulative IL-6 secretions indicated that a change in base concentration did not have a significant impact (Figure 6B). The two remaining formulations (0.175 M and 0.1 M at 50 wt%) possessed similar swelling and degradation profiles, which were more strongly influenced by the initial water content than base concentration. Astrocyte reactivity against PEG hydrogels depend on the degradation rates, which in turn are dependent on water diffusing into the polymer network [57]. Astrocyte reactivities also depend on the degradation products and the scaffold material. As such, the immunoassay was conducted over the course of 15 days to capture the effect of the hydrogel degradation rate and degradation products on the immune response of the astrocytes. Since these properties were all consistent between the two formulations, the IL-6 secretions did not vary significantly between the two hydrogels. The degradation products did not further incite an increase in astrocyte reactivity, and the onset of degradation did not prolong inflammation, since IL-6 secretions plateaued when hydrogels began to slowly degrade on day 7. As expected, wounded NHA secreted significantly more IL-6 and exhibited an elevated immune response that was maintained throughout the duration of the study due to sustained astrocyte reactivity, as indicated by Figure 6A. These results conform with research conducted by East and colleagues, which had revealed astrocytes cultured as a monolayer on 2D surfaces exhibit a constitutively activated state with high levels of IL-6 secretion [58].

Astrocytes *in vivo* possess small 10 µm cell bodies and radially branched processes that connect to synapses [59]. GFAP is an intermediate filament in astrocytes which is upregulated during activation, as reactive astrocytes indicate neuroinflammation through higher quantitative

levels of the protein and morphological changes with hypertrophic cell bodies [57]. The immunocytochemistry experiments and confocal microscope imaging were also conducted over the course of 15 days to determine the effect of the hydrogel degradation on the astrocyte reactivity, both in terms of the cell morphology and GFAP. For both 0.175 M and 0.1 M hydrogels with 50 wt% water content, astrocytes on the hydrogel surface retained a round morphology. When natural ECM polymers like collagen are used in hydrogel cell culture models, astrocytes often retain their in vivo stellate morphology and express lower GFAP than in standard cell culture conditions on tissue culture treated surfaces of flasks and plates, since the microenvironment naturally supports a heterogenous population of astrocytes and in vivo phenotypic markers [60]. However, synthetic hydrogels reduce the stellate morphology of astrocytes and increase reactivity [61]. Previous research has shown that there is an optimal stiffness for hydrogels to adopt physiological morphologies, since soft hydrogels decrease the traction needed for astrocytes to extend their processes, while the matrix is difficult to deform in stiffer hydrogels [25]. Regardless, the hydrogels yielded astrocyte morphologies which more closely resembled their native state, since the mechanical cues from the control well plates forced astrocytes to adjust to flat surfaces and adopt defined shapes [62]. A round morphology and the presence of GFAP from NHA on the hydrogels indicated astrocyte reactivity [63]. The weak positive association between the normalized GFAP fluorescence and cell diameter is indicative of the hypertrophy upon NHA activation.

For both formulations, the normalized GFAP fluorescence intensities followed a similar timeline as the IL-6 secretions, indicating IL-6 release was linked to astrocyte reactivity.

Furthermore, NHA diameters and GFAP intensities began to decrease and plateau from day 5 and onwards after the highest values were reached by both formulations, as the NHA adjusted to

the hydrogel microenvironment. These results suggest the onset of degradation, including an enzymatic breakdown of hydrogels due to NHA and the degradation products, did not further incite or sustain astrocyte reactivity. The 0.1 M and 50 wt% hydrogel induced a significantly higher astrocyte reactivity than the 0.175 M hydrogel through its peak GFAP intensity on day 5 and peak astrocyte diameter on day 3. This finding can be attributed to the difference in storage moduli between the two formulations. Hu and colleagues observed hydrogels with a lower storage modulus have a higher astrocyte reactivity [64], since astrocytes cultured on stiff matrices express lower GFAP, while cells on soft matrices exhibit high GFAP levels. According to the rheology data (Figure 3A), the 0.1 M and 50 wt% hydrogels had an 85% lower storage modulus than 0.175 M and 50 wt% hydrogels. The immunocytochemistry data overall revealed the hydrogels were not inert and elicited a reactive astrocyte phenotype. The 0.175 M hydrogel at 50 wt% appears to be more biocompatible, as it induces a lower astrocyte reactivity than the 0.1 M hydrogel. Astrocyte reactivity can potentially be beneficial, as Bjugstad and colleagues suggest inducing the reactive astrocyte phenotype can be a therapeutic strategy during brain cancer treatment by reducing the population of tumor associated astrocyte phenotypes that make tumors more malignant [57].

The motivation for this study was to characterize the hydrogel properties and determine the most optimal formulation for compatibility toward GBM treatment. The overall findings have indicated that the thiol-Michael addition hydrogel with 0.175 M NaHCO₃ and 50 wt% water content is the most compatible mechanically, chemically, and biologically with the GBM microenvironment. This formulation will thus be a suitable injectable hydrogel platform for GBM therapy. Although soft hydrogel matrices less than 1 kPa can enhance the hydrogel-tissue interface and contact area in the brain for optimal drug delivery applications [65, 66], stiffer

materials have been demonstrated to promote GBM invasion through expression of CD44 and matrix metalloproteinases such as MMP-2 [67]. Hence, hydrogels that possess storage moduli and stiffnesses higher than soft brain tissue may help to promote GBM migration into the material for subsequent entrapment, as is proposed for our future application of this hydrogel platform. However, more research efforts are needed to develop this hydrogel platform further for capturing GBM cells. For example, Solano and colleagues had demonstrated that a sodiumalginate based macroporous hydrogel both with and without RGD cell-adhesion peptides grafted on the surface enabled F98 GBM cells to invade into the matrix [68]. Previous research had also shown thiol-acrylate injectable hydrogels can be functionalized with oligolysine peptides to promote cell attachment to the surface [21]. The hydrogel pores can therefore be tuned and/or the hydrogel surfaces can potentially be functionalized with affinity ligands to help promote GBM migration into the matrices. Future research will also entail conducting *in vivo* studies to determine the immune responses of the hydrogel implants in an orthotopic rodent model and the role that the interstitial fluid flow may play in the GBM migration and invasion into the material [69].

Conclusions

The results from this study indicated that a PEGDA-Thiocure injectable hydrogel with 50 wt% water content and 0.175 M NaHCO_{3(aq)} is an optimal platform for physical, chemical, and biological compatibility toward GBM therapy. This formulation swells minimally and slowly over time and can potentially mitigate damage to healthy neurons upon implantation in the resection cavity. It possesses a sufficiently crosslinked network and can reduce the risk of leaching soluble components into the GBM resection bed. Its storage modulus is ideal for withstanding the high intracranial pressures associated with GBM, while also avoiding a tissue

mechanical mismatch. The hydrogel is biodegradable, yet stable over the course of two weeks and can potentially be used for chronic implantation. Furthermore, this formulation is biocompatible with astrocytes and elicits a low immunogenic response. It induces astrocytes to secrete small levels of IL-6, which can potentially attract GBM migration and invasion toward the hydrogel in the resection cavity. The astrocyte reactivity stabilizes after 5 days, and the onset of degradation does not incite further immunogenicity. Overall, this platform is a promising biomaterial for compatibility toward GBM therapy. This injectable hydrogel platform will be developed further to entrap and eradicate GBM cells with chemical and physical stimuli.

Acknowledgments

This research is supported by the NSF CAREER Award [Grant CBET-1652112] (SSV) as well as the NSERC Postgraduate Doctoral Scholar Award and P.E.O. Scholar Award (ZMK).

Disclosures

ZMK, SSV, TEL, and EV are inventors on a pending patent related to this work. The authors declare no other conflicts of interest or competing financial interests.

References

- [1] P. Puente, N. Fettig, M.J. Luderer, A. Jin, S. Shah, B. Muz, V. Kapoor, S.M. Goddu, N.N. Salama, C. Tsien, D. Thotala, K. Shoghi, B. Rogers, A.K. Azab, Injectable Hydrogels for Localized Chemotherapy and Radiotherapy in Brain Tumors, J Pharm Sci 107(3) (2018) 922-933.
- [2] P. De Bonis, C. Anile, A. Pompucci, A. Fiorentino, M. Balducci, S. Chiesa, L. Lauriola, G. Maira, A. Mangiola, The influence of surgery on recurrence pattern of glioblastoma, Clin Neurol Neurosurg 115(1) (2013) 37-43.
- [3] S.K. Singh, C. Hawkins, I.D. Clarke, J.A. Squire, J. Bayani, T. Hide, R.M. Henkelman, M.D. Cusimano, P.B. Dirks, Identification of human brain tumour initiating cells, Nature 432(7015) (2004) 396-401.
- [4] T. Glaser, I. Han, L. Wu, X. Zeng, Targeted Nanotechnology in Glioblastoma Multiforme, Front Pharmacol 8 (2017) 166.
- [5] L. Autier, A. Clavreul, M.L. Cacicedo, F. Franconi, L. Sindji, A. Rousseau, R. Perrot, C.N. Montero-Menei, G.R. Castro, P. Menei, A new glioblastoma cell trap for implantation after surgical resection, Acta Biomater 84 (2019) 268-279.
- [6] A. Jain, M. Betancur, G.D. Patel, C.M. Valmikinathan, V.J. Mukhatyar, A. Vakharia, S.B. Pai, B. Brahma, T.J. MacDonald, R.V. Bellamkonda, Guiding intracortical brain tumour cells to an extracortical cytotoxic hydrogel using aligned polymeric nanofibres, Nat Mater 13(3) (2014) 308-16.
- [7] J.G. Lyon, S.L. Carroll, N. Mokarram, R.V. Bellamkonda, Electrotaxis of Glioblastoma and Medulloblastoma Spheroidal Aggregates, Scientific Reports 9(1) (2019) 5309.
- [8] C. Edsall, Z.M. Khan, L. Mancia, S. Hall, W. Mustafa, E. Johnsen, A.L. Klibanov, Y.Y. Durmaz, E. Vlaisavljevich, Bubble Cloud Behavior and Ablation Capacity for Histotripsy Generated from Intrinsic or Artificial Cavitation Nuclei, Ultrasound Med Biol 47(3) (2021) 620-639.

- [9] J.R. Sukovich, C.A. Cain, A.S. Pandey, N. Chaudhary, S. Camelo-Piragua, S.P. Allen, T.L. Hall, J. Snell, Z. Xu, J.M. Cannata, D. Teofilovic, J.A. Bertolina, N. Kassell, Z. Xu, In vivo histotripsy brain treatment, Journal of neurosurgery (2018) 1-8.
- [10] J.R. Sukovich, C.A. Cain, A.S. Pandey, N. Chaudhary, S. Camelo-Piragua, S.P. Allen, T.L. Hall, J. Snell, Z. Xu, J.M. Cannata, D. Teofilovic, J.A. Bertolina, N. Kassell, Z. Xu, In vivo histotripsy brain treatment, J Neurosurg (2018) 1-8.
- [11] C. Echalier, L. Valot, J. Martinez, A. Mehdi, G. Subra, Chemical cross-linking methods for cell encapsulation in hydrogels, Materials Today Communications 20 (2019) 100536.
- [12] K.R. Coogan, P.T. Stone, N.D. Sempertegui, S.S. Rao, Fabrication of micro-porous hyaluronic acid hydrogels through salt leaching, European Polymer Journal 135 (2020).
- [13] K. Shah, D. Vasileva, A. Karadaghy, S.P. Zustiak, Development and characterization of polyethylene glycol–carbon nanotube hydrogel composite, Journal of Materials Chemistry B 3(40) (2015) 7950-7962.
- [14] D.P. Nair, M. Podgórski, S. Chatani, T. Gong, W. Xi, C.R. Fenoli, C.N. Bowman, The Thiol-Michael Addition Click Reaction: A Powerful and Widely Used Tool in Materials Chemistry, Chemistry of Materials 26(1) (2013) 724-744.
- [15] R.G. Chapman, E. Ostuni, M.N. Liang, G. Meluleni, E. Kim, L. Yan, G. Pier, H.S. Warren, G.M. Whitesides, Polymeric Thin Films That Resist the Adsorption of Proteins and the Adhesion of Bacteria, Langmuir 17(4) (2001) 1225-1233.
- [16] N.G. Moon, A.M. Pekkanen, T.E. Long, T.N. Showalter, B. Libby, Thiol-Michael 'click' hydrogels as an imageable packing material for cancer therapy, Polymer 125 (2017) 66-75.
- [17] A.H. Khan, J.K. Cook, W.J. Wortmann, 3rd, N.D. Kersker, A. Rao, J.A. Pojman, A.T. Melvin, Synthesis and characterization of thiol-acrylate hydrogels using a base-catalyzed Michael addition for 3D cell culture applications, J Biomed Mater Res B Appl Biomater 108(5) (2020) 2294-2307.
- [18] M.S. Peach, J. Moore, W. Giles, J. Trainor, T. Long, N. Moon, J.E. Hylton, T.N. Showalter, B. Libby, Development and preclinical testing of a novel biodegradable hydrogel vaginal packing technology for gynecologic high-dose-rate brachytherapy, J Contemp Brachytherapy 10(4) (2018) 306-314.
- [19] J. Karvinen, T.O. Ihalainen, M.T. Calejo, I. Jönkkäri, M. Kellomäki, Characterization of the microstructure of hydrazone crosslinked polysaccharide-based hydrogels through rheological and diffusion studies, Materials Science and Engineering: C 94 (2019) 1056-1066.
- [20] R. Suriano, G. Griffini, M. Chiari, M. Levi, S. Turri, Rheological and mechanical behavior of polyacrylamide hydrogels chemically crosslinked with allyl agarose for two-dimensional gel electrophoresis, Journal of the Mechanical Behavior of Biomedical Materials 30 (2014) 339-346.
- [21] C.D. Pritchard, T.M. O'Shea, D.J. Siegwart, E. Calo, D.G. Anderson, F.M. Reynolds, J.A. Thomas, J.R. Slotkin, E.J. Woodard, R. Langer, An injectable thiol-acrylate poly(ethylene glycol) hydrogel for sustained release of methylprednisolone sodium succinate, Biomaterials 32(2) (2011) 587-97.
- [22] N. Wang, F. Yao, K. Li, L. Zhang, G. Yin, M. Du, B. Wu, Fisetin regulates astrocyte migration and proliferation in vitro, Int J Mol Med 39(4) (2017) 783-790.
- [23] J.W. Ivey, E.L. Latouche, M.B. Sano, J.H. Rossmeisl, R.V. Davalos, S.S. Verbridge, Targeted cellular ablation based on the morphology of malignant cells, Scientific Reports 5(1) (2015) 17157.
- [24] S. Galarza, A.J. Crosby, C. Pak, S.R. Peyton, Control of Astrocyte Quiescence and Activation in a Synthetic Brain Hydrogel, Advanced Healthcare Materials 9(4) (2020) 1901419.
- [25] A.L. Placone, P.M. McGuiggan, D.E. Bergles, H. Guerrero-Cazares, A. Quiñones-Hinojosa, P.C. Searson, Human astrocytes develop physiological morphology and remain quiescent in a novel 3D matrix, Biomaterials 42 (2015) 134-43.
- [26] P. Panyamao, W. Ruksiriwanich, P. Sirisa-Ard, S. Charumanee, Injectable Thermosensitive Chitosan/Pullulan-Based Hydrogels with Improved Mechanical Properties and Swelling Capacity, Polymers 12(11) (2020) 2514.

- [27] P.J. Scott, V. Meenakshisundaram, N.A. Chartrain, J.M. Sirrine, C.B. Williams, T.E. Long, Additive Manufacturing of Hydrocarbon Elastomers via Simultaneous Chain Extension and Cross-linking of Hydrogenated Polybutadiene, ACS Applied Polymer Materials 1(4) (2019) 684-690.
- [28] S.L. Blackburn, M.D. Smyth, Hydrogel-induced cervicomedullary compression after posterior fossa decompression for Chiari malformation. Case report, J Neurosurg 106(4 Suppl) (2007) 302-4.
- [29] I. Roy, M.N. Gupta, Smart Polymeric Materials: Emerging Biochemical Applications, Chemistry & Biology 10(12) (2003) 1161-1171.
- [30] A. Baldwin, L. Yu, E. Meng, An Electrochemical Impedance-Based Thermal Flow Sensor for Physiological Fluids, Journal of Microelectromechanical Systems 25(6) (2016) 1015-1024.
- [31] S.R. Caliari, J.A. Burdick, A practical guide to hydrogels for cell culture, Nature Methods 13(5) (2016) 405-414.
- [32] E. Hasanzadeh, S. Ebrahimi-Barough, E. Mirzaei, M. Azami, S.M. Tavangar, N. Mahmoodi, A. Basiri, J. Ai, Preparation of fibrin gel scaffolds containing MWCNT/PU nanofibers for neural tissue engineering, J. Biomed Mater Res A 107(4) (2019) 802-814.
- [33] M. Basan, T. Risler, J.F. Joanny, X. Sastre-Garau, J. Prost, Homeostatic competition drives tumor growth and metastasis nucleation, Hfsp j 3(4) (2009) 265-72.
- [34] B. Delpech, C. Maingonnat, N. Girard, C. Chauzy, R. Maunoury, A. Olivier, J. Tayot, P. Creissard, Hyaluronan and hyaluronectin in the extracellular matrix of human brain tumour stroma, Eur J Cancer 29a(7) (1993) 1012-7.
- [35] K. Franze, The mechanical control of nervous system development, Development 140(15) (2013) 3069-77.
- [36] C. Wang, X. Tong, F. Yang, Bioengineered 3D Brain Tumor Model To Elucidate the Effects of Matrix Stiffness on Glioblastoma Cell Behavior Using PEG-Based Hydrogels, Molecular Pharmaceutics 11(7) (2014) 2115-2125.
- [37] J. da Silva, F. Lautenschläger, E. Sivaniah, J.R. Guck, The cavity-to-cavity migration of leukaemic cells through 3D honey-combed hydrogels with adjustable internal dimension and stiffness, Biomaterials 31(8) (2010) 2201-2208.
- [38] M.J. Moura, M.M. Figueiredo, M.H. Gil, Rheological Study of Genipin Cross-Linked Chitosan Hydrogels, Biomacromolecules 8(12) (2007) 3823-3829.
- [39] P.B. Welzel, S. Prokoph, A. Zieris, M. Grimmer, S. Zschoche, U. Freudenberg, C. Werner, Modulating Biofunctional starPEG Heparin Hydrogels by Varying Size and Ratio of the Constituents, Polymers 3(1) (2011) 602-620.
- [40] T.J. Grundy, E. De Leon, K.R. Griffin, B.W. Stringer, B.W. Day, B. Fabry, J. Cooper-White, G.M. O'Neill, Differential response of patient-derived primary glioblastoma cells to environmental stiffness, Scientific Reports 6(1) (2016) 23353.
- [41] C. Schmitt, V. Adamski, F. Rasch, R. Adelung, R. Lucius, M. Synowitz, K. Hattermann, J. Held-Feindt, Establishment of a glioblastoma in vitro (in)complete resection dual co-culture model suitable for drug testing, Annals of Anatomy Anatomischer Anzeiger 228 (2020) 151440.
- [42] T.M. O'Shea, A.A. Aimetti, E. Kim, V. Yesilyurt, R. Langer, Synthesis and characterization of a library of in-situ curing, nonswelling ethoxylated polyol thiol-ene hydrogels for tailorable macromolecule delivery, Adv Mater 27(1) (2015) 65-72.
- [43] A. Metters, J. Hubbell, Network formation and degradation behavior of hydrogels formed by Michael-type addition reactions, Biomacromolecules 6(1) (2005) 290-301.
- [44] M. Zhao, F. Danhier, C. Bastiancich, N. Joudiou, L.P. Ganipineni, N. Tsakiris, B. Gallez, A.D. Rieux, A. Jankovski, J. Bianco, V. Preat, Post-resection treatment of glioblastoma with an injectable nanomedicine-loaded photopolymerizable hydrogel induces long-term survival, International journal of pharmaceutics 548(1) (2018) 522-529.

- [45] I. Zur, T. Tzuk-Shina, M. Guriel, A. Eran, O. Kaidar-Person, Survival impact of the time gap between surgery and chemo-radiotherapy in Glioblastoma patients, Scientific Reports 10(1) (2020) 9595.
- [46] C.M. Bellettato, M. Scarpa, Possible strategies to cross the blood–brain barrier, Italian Journal of Pediatrics 44(2) (2018) 131.
- [47] B.P. Mead, P. Mastorakos, J.S. Suk, A.L. Klibanov, J. Hanes, R.J. Price, Targeted gene transfer to the brain via the delivery of brain-penetrating DNA nanoparticles with focused ultrasound, J Control Release 223 (2016) 109-117.
- [48] M.F. Lorenzo, S.C. Thomas, Y. Kani, J. Hinckley, M. Lee, J. Adler, S.S. Verbridge, F.-C. Hsu, J.L. Robertson, R.V. Davalos, J.H. Rossmeisl, Jr., Temporal Characterization of Blood-Brain Barrier Disruption with High-Frequency Electroporation, Cancers (Basel) 11(12) (2019) 1850.
- [49] T. Showalter, T.E. Long, N. Moon, Thiol-Michael Addition Hydrogel-Based Brachytherapy System and Methods Comprising the Same in: U.o. Virginia (Ed.) United States 2017, p. 65.
- [50] A.D. Gilmour, A.J. Woolley, L.A. Poole-Warren, C.E. Thomson, R.A. Green, A critical review of cell culture strategies for modelling intracortical brain implant material reactions, Biomaterials 91 (2016) 23-43
- [51] E.M. Wilts, A. Gula, C. Davis, N. Chartrain, C.B. Williams, T.E. Long, Vat photopolymerization of liquid, biodegradable PLGA-based oligomers as tissue scaffolds, European Polymer Journal 130 (2020) 109693.
- [52] V. Kasymov, O. Larina, C. Castaldo, N. Marina, M. Patrushev, S. Kasparov, A.V. Gourine, Differential sensitivity of brainstem versus cortical astrocytes to changes in pH reveals functional regional specialization of astroglia, J Neurosci 33(2) (2013) 435-41.
- [53] A.-G.S. Group, EXTENT OF RESECTION AND SURVIVAL IN GLIOBLASTOMA MULTIFORME: IDENTIFICATION OF AND ADJUSTMENT FOR BIAS, Neurosurgery 62(3) (2008) 564-576.
- [54] H. Zhang, Y. Zhou, B. Cui, Z. Liu, H. Shen, Novel insights into astrocyte-mediated signaling of proliferation, invasion and tumor immune microenvironment in glioblastoma, Biomed Pharmacother 126 (2020) 110086.
- [55] R. Li, G. Li, L. Deng, Q. Liu, J. Dai, J. Shen, J. Zhang, IL-6 augments the invasiveness of U87MG human glioblastoma multiforme cells via up-regulation of MMP-2 and fascin-1, Oncol Rep 23(6) (2010) 1553-9.
- [56] B.H. Rath, J.M. Fair, M. Jamal, K. Camphausen, P.J. Tofilon, Astrocytes enhance the invasion potential of glioblastoma stem-like cells, PLoS One 8(1) (2013) e54752.
- [57] K.B. Bjugstad, K. Lampe, D.S. Kern, M. Mahoney, Biocompatibility of poly(ethylene glycol)-based hydrogels in the brain: an analysis of the glial response across space and time, J Biomed Mater Res A 95(1) (2010) 79-91.
- [58] E. East, J.P. Golding, J.B. Phillips, A versatile 3D culture model facilitates monitoring of astrocytes undergoing reactive gliosis, J Tissue Eng Regen Med 3(8) (2009) 634-46.
- [59] N.A. Oberheim, T. Takano, X. Han, W. He, J.H. Lin, F. Wang, Q. Xu, J.D. Wyatt, W. Pilcher, J.G. Ojemann, B.R. Ransom, S.A. Goldman, M. Nedergaard, Uniquely hominid features of adult human astrocytes, J Neurosci 29(10) (2009) 3276-87.
- [60] S. Balasubramanian, J.A. Packard, J.B. Leach, E.M. Powell, Three-Dimensional Environment Sustains Morphological Heterogeneity and Promotes Phenotypic Progression During Astrocyte Development, Tissue Eng Part A 22(11-12) (2016) 885-98.
- [61] C. Papadimitriou, H. Celikkaya, M.I. Cosacak, V. Mashkaryan, L. Bray, P. Bhattarai, K. Brandt, H. Hollak, X. Chen, S. He, C.L. Antos, W. Lin, A.K. Thomas, A. Dahl, T. Kurth, J. Friedrichs, Y. Zhang, U. Freudenberg, C. Werner, C. Kizil, 3D Culture Method for Alzheimer's Disease Modeling Reveals Interleukin-4 Rescues $A\beta42$ -Induced Loss of Human Neural Stem Cell Plasticity, Dev Cell 46(1) (2018) 85-101.e8.
- [62] J. Lee, M.J. Cuddihy, N.A. Kotov, Three-dimensional cell culture matrices: state of the art, Tissue Eng Part B Rev 14(1) (2008) 61-86.

- [63] S.S. Rao, J. DeJesus, A.R. Short, J.J. Otero, A. Sarkar, J.O. Winter, Glioblastoma Behaviors in Three-Dimensional Collagen-Hyaluronan Composite Hydrogels, ACS Applied Materials & Interfaces 5(19) (2013) 9276-9284.
- [64] Y. Hu, G. Huang, J. Tian, J. Qiu, Y. Jia, D. Feng, Z. Wei, S. Li, F. Xu, Matrix stiffness changes affect astrocyte phenotype in an in vitro injury model, NPG Asia Materials 13(1) (2021) 35.
- [65] M.J. Rowland, C.C. Parkins, J.H. McAbee, A.K. Kolb, R. Hein, X.J. Loh, C. Watts, O.A. Scherman, An adherent tissue-inspired hydrogel delivery vehicle utilised in primary human glioma models, Biomaterials 179 (2018) 199-208.
- [66] A. Belousov, S. Titov, N. Shved, M. Garbuz, G. Malykin, V. Gulaia, A. Kagansky, V. Kumeiko, The Extracellular Matrix and Biocompatible Materials in Glioblastoma Treatment, Frontiers in Bioengineering and Biotechnology 7(341) (2019).
- [67] A.E. Erickson, S.K. Lan Levengood, J. Sun, F.C. Chang, M. Zhang, Fabrication and Characterization of Chitosan-Hyaluronic Acid Scaffolds with Varying Stiffness for Glioblastoma Cell Culture, Adv Healthc Mater 7(15) (2018) e1800295.
- [68] A.G. Solano, J. Dupuy, H. Therriault, B. Liberelle, N. Faucheux, M.-A. Lauzon, N. Virgilio, B. Paquette, An alginate-based macroporous hydrogel matrix to trap cancer cells, Carbohydrate Polymers 266 (2021) 118115.
- [69] J.M. Munson, R.V. Bellamkonda, M.A. Swartz, Interstitial flow in a 3D microenvironment increases glioma invasion by a CXCR4-dependent mechanism, Cancer Res 73(5) (2013) 1536-46.